Progress In Electromagnetics Research C, Vol. 112, 221–238, 2021

Compact-Size Quad-Band Patch and MIMO Antenna System for 5G Mobile Handsets

May A. El-Hassan*, Asmaa E. Farahat, and Khalid F. A. Hussein

Abstract—A compact-size quad-band (28/45/51/56 GHz) microstrip patch antenna is proposed for the Fifth Generation (5G) mobile handsets. The present paper introduces a new method to reduce the size of a 28-GHz rhombic patch antenna so as to properly operate at the higher frequency bands (45/51/56 GHz) without negative effects on the antenna characteristics at 28 GHz. A novel design is introduced for the quad-band patch antenna to include complicated radiation mechanisms required for multiple-band operation. The proposed (single-element) antenna is constructed as primary and secondary patches which are capacitively coupled and designed to realize impedance matching and to produce appropriate radiation patterns in the four frequency bands. Two-port and four-port MIMO antenna systems that employ the quad-band patch antenna are proposed in the present work for the 5G mobile handsets. Numerical and experimental investigations are achieved to assess the performance of both the single-element antenna and proposed MIMO antenna systems including the return loss at each antenna port and the coupling coefficients between different ports. It is shown that the simulation results agree with the experimental measurements, and both show good performance. The bandwidths achieved around 28, 45, 51, and 56 GHz are about 0.6, 2.0, 1.8, and 1.3 GHz, respectively. The radiation patterns produced when each port is excited alone are shown to be suitable for spatial diversity scheme with high radiation efficiency. It is shown that the envelope correlation coefficient (ECC) and diversity gain (DG) are perfect over the four frequency bands.

1. INTRODUCTION

Fifth Generation (5G) is a new technology of mobile communications, which introduces the Internet of Things (IOTs) into the network of devices (D2D communications) with wider bandwidth, higher data rates, and better coverage, and facilitates the solution of some serious problems such as latency and security in mobile communications [1]. The spectrum allocation is a matter of great concern in the 5G mobile communications. The unused millimeter-wave (mm-wave) electromagnetic spectrum (30–300 GHz) has attracted attention and has been introduced as a candidate for the 5G mobile communication to enable multi-Gbit/s transmission rate exploiting the wide available bandwidth to meet the demands of the future applications which require high quality and low latency transmission, and hence, it is able to handle much greater capacity than the available 4G networks.

The mm-wave frequency bands centered at 28, 38, 60, and 73 GHz have been allocated for 5G mobile communications by International Telecommunications Union (ITU) [2]. Bands of 59–64 GHz are allocated by the Federal Communications Commission (FCC) as an unlicensed band for short range and wireless communications of high speeds [3, 4]. Some of the expected mm-wave bands recommended for 5G mobile communications are: 27.5–29.5 GHz, 33.4–36 GHz, 37–40.5 GHz, 42–45 GHz, 47–50.2 GHz, 50.4–52.6 GHz, and 59.3–71 GHz [1]. Significant attenuation is caused by oxygen molecules in the atmosphere to react with mm-wave signals and reaches up to 10 dB/km especially for the frequencies

Received 8 March 2021, Accepted 6 May 2021, Scheduled 17 May 2021
* Corresponding author: May Abd El-Azem Abo-Elhassan (mayaboelhassan@yahoo.com).
The authors are with the Electronics Research Institute (ERI), Cairo, Egypt.

higher than 45 GHz. Due to this defect, it is not recommended to operate at frequencies that are much higher than 45 GHz for communication applications and long-range radar. For cellular mobile communications, the 28 GHz band is advantageous due to its low oxygen absorption rates unlike the higher mm-wave frequencies especially in 60 GHz band. The operation in the frequency bands higher than 45 GHz is recommended for short-range communications such as Wi-Fi (with the WiGiG standard in the 60-GHz band) [1, 5].

Due to the short wavelength of mm-waves, the employment of spatial, pattern and polarization diversity techniques, such as Multi-Input Multi-Output (MIMO), is highly recommended for future generations of wireless communication systems that enable several Gb/s communication speed. In a MIMO antenna system, high radiation efficiency and high isolation between the multiple ports are required [6]. Employing MIMO antenna systems mitigates channel fading problems and generally enhances the performance of the wireless communication systems [7].

Recently, a lot of research work has provided many designs for single-element antenna as well as MIMO antenna systems for 5G mobile handsets. For example, the work of [3] introduces a 60-GHz antenna which consists of H-shaped and E-shaped slots on the radiating patch. The work of [1] presents a dual-band circular microstrip patch antenna with an elliptical slot. This antenna operates at frequencies of 28 GHz and 45 GHz, with bandwidths of 1.3 GHz and 1 GHz. In [6], a printed planar Yagi-Uda antenna is introduced for dual-band operation at 28/38 GHz. In the same work, a four-port MIMO antenna system is constructed using the proposed Yagi-Uda antenna arranged at the edges of the mobile handset to provide pattern and polarization diversities. In [8], a 28-GHz four-port MIMO antenna is proposed, where each antenna has an end-fire gain to provide pattern and polarization diversities. The work of [9] introduces a compact microstrip line fed dual-band printed four-port MIMO antennas resonating at 28 GHz and 38 GHz to provide spatial diversity. In [10], a compact dual-band (38/60 GHz) microstrip patch antenna is proposed for 5G mobile handsets. In [11], a dual-band (38/54 GHz) microstrip patch antenna and a 4-element array are proposed to achieve 12 dB gain for 5G mobile data applications. The work of [12] presents a compact MIMO antenna design with polarization and pattern diversity operating in the frequency band (34–38 GHz).

In the present work, a new method is introduced to modify the design of a rhombic patch antenna that works at 28 GHz as its first-order resonance efficiently radiates at the desired multiple higher frequency bands with appropriate shape of the radiation patterns and reasonable values of the maximum gain. The principal idea to achieve this is to reduce the area of the conducting surface of such a rhombic patch so as to prevent the formation of higher-order patterns of the surface current at the desired higher frequencies and, thereby, preventing the nulls in the radiation patterns. Definitely, this reduction of the patch surface should be done without badly affecting its performance at the principle resonant frequency (28 GHz). This can be performed by appropriately making some cuts in its geometry to remove the regions of negligible magnitude of the patch surface current formed at 28 GHz. In this way, the size of the patch antenna is significantly reduced while its performance is kept at 28 GHz almost the same as the originally designed rhombic antenna. The smaller size of the geometrically modified patch antenna allows the excitation of higher-order resonances at higher frequencies with significantly improved shapes of the radiation patterns and acceptable values of the gain. The development stages of the proposed patch antenna design to get it operating in the above mentioned four frequency bands are demonstrated in some detail. Moreover, to get the higher order resonances located at the desired frequency bands, a parasitic patch of the appropriate geometry is capacitively coupled to the 28-GHz patch. The load impedance caused by such a reactively coupled patch controls the locations of the three higher-order resonant frequencies.

In this way, the present work arrives at a novel design for a (28/45/51/56 GHz) quad-band microstrip patch antenna for 5G mobile phones. The operation of the proposed antenna in such multiple bands is requested to use the currently available allocated 5G spectra in a single system. The proposed antenna can be viewed as composed of two patches; the primary patch is inset-fed by a microstrip line whereas the secondary patch is fed through reactive coupling to the primary patch. The dimensions of the primary patch are set so that the patch operates in its first-order mode at 28 GHz. The higher-order resonances of the combined structure of the printed antenna (both primary and secondary patches) enable the radiation at the higher frequency bands (45/51/56 GHz).

Moreover, the present work proposes two-port and four-port MIMO antenna systems for operation

in the quad-band (28/45/51/56 GHz). The MIMO antenna performance including the return loss at each antenna port and the coupling coefficients between the different ports is investigated and shown to be suitable for 5G mobile communications. The radiation patterns produced when each port is excited alone are shown to be suitable for an efficient diversity scheme. The performance measures such as the envelope correlation coefficient (ECC) and diversity gain (DG) are evaluated showing excellent performance of the proposed MIMO antenna systems.

The remaining part of the present paper is organized as follows. Section 2 provides a detailed explanation of the development stages of the reduced-size patch antenna design to radiate at 28 GHz. Section 3 gives a description of the final design and mechanism of operation of the quad-band microstrip patch antenna proposed for 5G mobile handsets. Section 4 proposes two- and four-port MIMO antenna systems that employ spatial diversity for enhancement of the wireless channel performance. Section 5 gives a summary of the proposed antenna performance and comparisons with some published designs. Finally, Section 6 provides the most important conclusions for the present work.

2. DEVELOPMENT OF A DESIGN FOR COMPACT-SIZE PATCH ANTENNA AT 28 GHz

In this section, the development stages of the proposed patch antenna design to get it operating in the four frequency bands at 28, 45, 51, and 56 GHz are demonstrated in some detail.

First, a rhombic patch antenna with right-angle corners is designed to operate at 28 GHz. If this patch is used to radiate at its higher-order resonances, the resulting radiation patterns and gain may not be appropriate for mobile applications due to the existing nulls and sidelobes. This is because the size of the 28-GHz patch is electrically large at the mm-wave frequencies higher than 28 GHz. It is expected that the higher the order of the radiating mode is, the larger numbers of the nulls and sidelobes of the radiation pattern are. The relatively large size of the conducting patch surface allows the formation of surface current patterns that result in radiation patterns with a number of nulls and sidelobes depending on the radiating mode order. Thus, if the area of the conducting patch surface is reduced the formed surface current patterns may result in acceptable shape of the radiation pattern and the maximum gain. The reduction of the area of the conducting surface of a rhombic patch (originally designed to radiate at 28 GHz) should not badly affect its performance at the principle resonant frequency (28 GHz). This can be performed by making some cuts in its geometry to remove the regions of negligible magnitude of the patch surface current formed at 28 GHz.

2.1. Conventional Design of Rhombic Patch Antenna at 28 GHz

The rhombic patch operating at 28 GHz has the dimensions shown in Figure 1(a). The patch is printed on a Rogers RO3003 substrate of height $h = 0.25$ mm, dielectric constant $\varepsilon_r = 3$, and loss tangent $\tan\delta = 0.001$ with a solid ground plane on the bottom of the substrate. To get the input impedance of this rhombic patch antenna matched to 50 Ω source, it is fed through a microstrip line with inset length

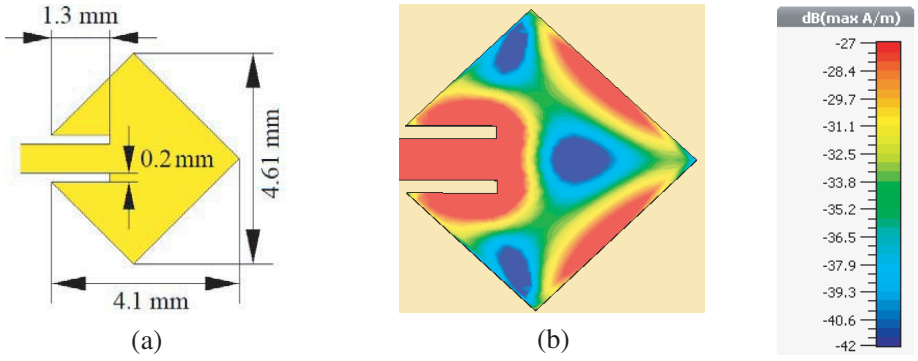

Figure 1. Rhombic patch antenna designed to operate at 28 GHz. (a) Dimensions of the patch antenna, (b) distribution of the surface current magnitude.

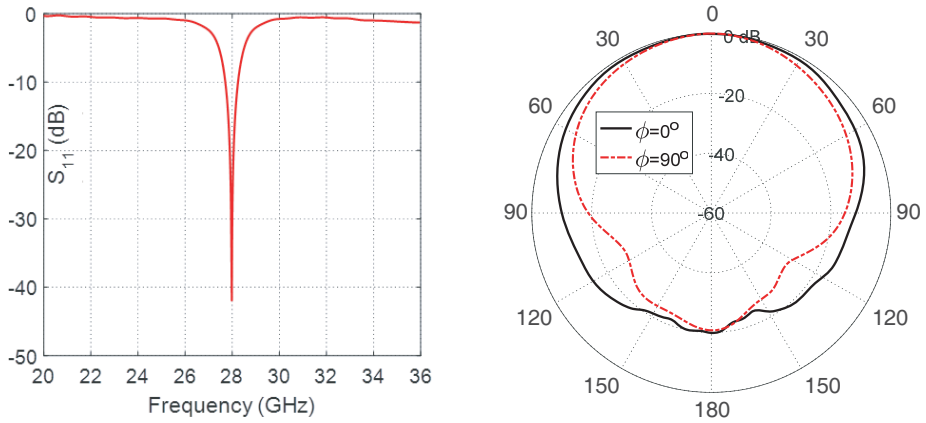

(a) (b)

Figure 2. Simulation results for the rhombic patch antenna. (a) Frequency response of $|S_{11}|$, (b) radiation patterns in the elevation planes at the patch resonance.

of 1.3 mm. This antenna has the distribution of the surface current magnitude presented in Figure 1(b). The frequency dependence of $|S_{11}|$ is presented in Figure 2(a), and the elevation radiation patterns are presented in Figure 2(b). The maximum antenna gain is 6.38 dBi.

In view of the current distribution on the surface of the rhombic patch, presented in Figure 1(b), it can be clear that the patch size can be significantly reduced by making some cuts in its geometry to remove the regions with negligible magnitude of the surface current without affecting the antenna characteristics at 28 GHz. However, the suggested cuts will be made in steps so as to study the effect of the geometrical modification made in each step on the antenna characteristics and to take the appropriate decisions for the cuts that should be made in the next step of the geometrical modifications.

2.2. Reduction of the Rhombic Patch Antenna Size

As shown in Figure 1(b), the central area of the patch and the regions near the upper and lower corners have negligible surface current. The regions near the patch corners can be removed by blending the corners with a suitable radius (0.5 mm) as shown in Figure 3(a). This modification reduces the

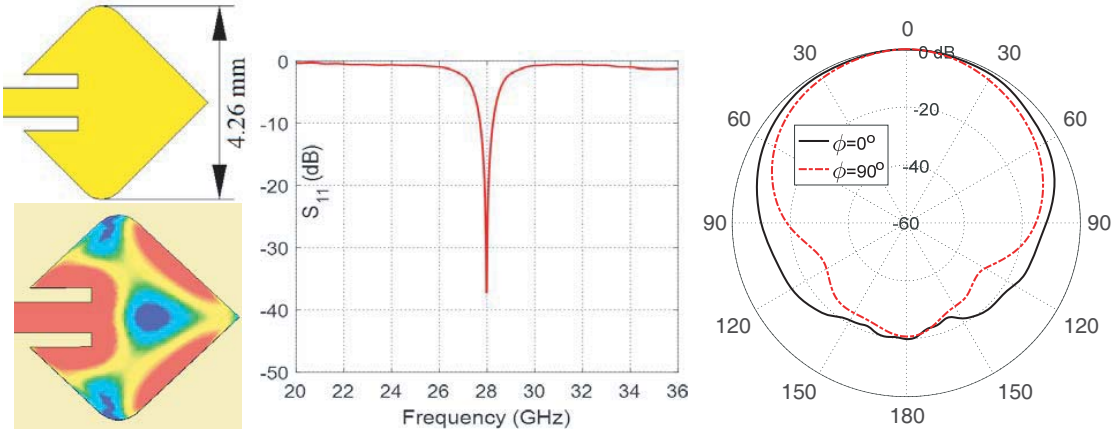

(a) (b) (c)

Figure 3. Design of rhombic patch antenna with blended corners. (a) The patch dimensions and the surface current distribution at the patch resonance, (b) the frequency response of $|S_{11}|$, (c) the radiation patterns in the elevation planes at the patch resonance.

vertical dimension of the patch to 4.26 mm, which is about 90% of the corresponding dimension of the original patch (4.61 mm). To keep the modified patch resonant at 28 GHz, the inset length is changed to 1.2 mm. The modified rhombic patch antenna presented in Figure 3(a) has the surface current distribution, $|S_{11}|$ frequency response, and elevation radiation patterns presented in Figures 3(a), 3(b), and 3(c), respectively. The maximum antenna gain is 6.38 dBi.

As shown in Figure 3(a), the surface current is very weak in the region of the patch near the midway between the location of the inset feed and the right-hand corner of the patch. Thus, for further reduction of the rhombic patch size, a circular sectorial aperture is cut to remove this region as shown in Figure 4(a). This modification reduces the vertical dimension of the patch to 3.91 mm, which is about 80% of the original rhombic patch dimension. To keep the modified patch resonant at 28 GHz, the inset length is changed to 1.32 mm. The modified rhombic patch antenna presented in Figure 4(a) has the surface current distribution, $|S_{11}|$ frequency response, and elevation radiation patterns presented in Figures 4(a), 4(b), and 4(c), respectively. The maximum antenna gain is 6.4 dBi.

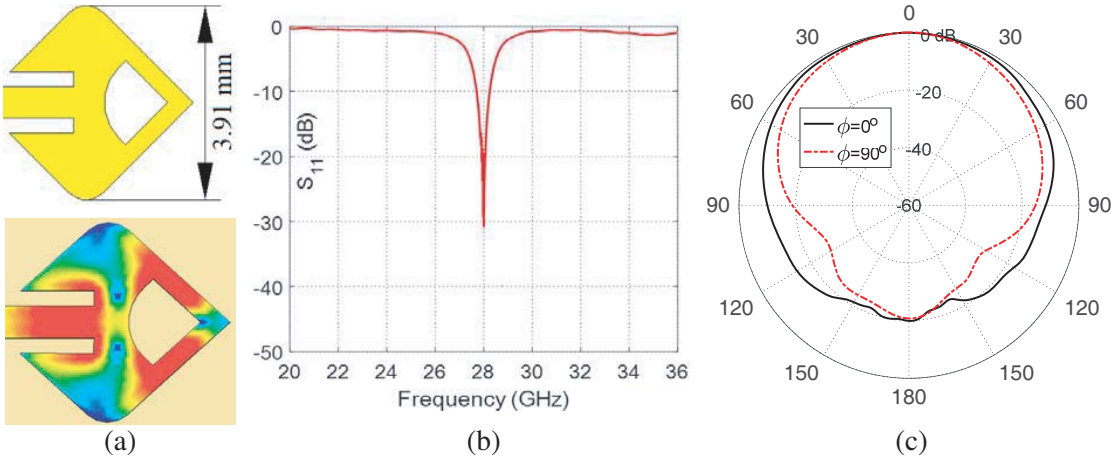

Figure 4. Design of rhombic patch antenna with blended corners and circular sectorial cut. (a) The patch dimensions and the surface current distribution at the patch resonance, (b) the frequency response of $|S_{11}|$, (c) the radiation patterns in the elevation planes at the patch resonance.

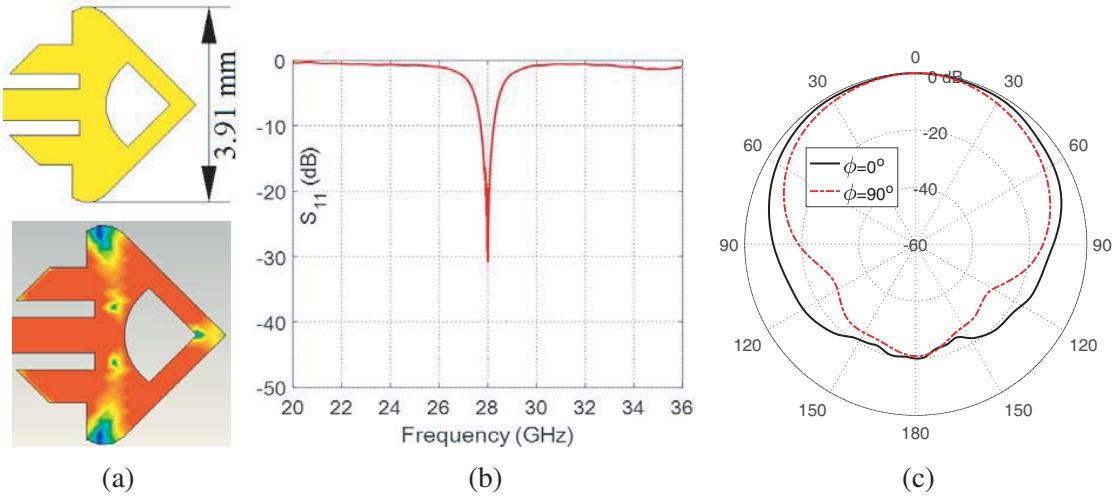

Figure 5. Final design of the 28-GHz compact-size patch antenna. (a) The patch dimensions and the surface current distribution at the patch resonance, (b) the frequency response of $|S_{11}|$, (c) the radiation patterns in the elevation planes at the patch resonance.

As shown in Figure 4(a), the surface current is very weak in the region of the patch near the blended corners of the patch. Thus, for further reduction of the rhombic patch size, two triangular cuts are made to remove these regions as shown in Figure 5(a). Upon this modification the area of the conducting surface of the final patch is reduced to about 65% of the original rhombic patch size. To keep the modified patch resonant at 28 GHz, the inset length is changed to 1.34 mm. The modified patch antenna presented in Figure 5(a) has the surface current distribution, $|S_{11}|$ frequency response, and elevation radiation patterns presented in Figures 5(a), 5(b), and 5(c), respectively. The maximum antenna gain produced by the patch with its final design is about 6.4 dBi.

In this way, the size of the patch antenna is significantly reduced while its performance is kept almost the same. This can be clear by comparison between the frequency response of the reflection coefficient and the radiation patterns of the modified patch with its final design (shown in Figure 5) to those of the original rhombic patch (shown in Figure 2). The key principle of this achievement is that the blends and cuts are made to remove the regions of the original rhombic patch where the surface current is very weak and can be negligible. Such a reduced-size patch can be further modified to resonate at higher frequencies; this is explained in the following section of the present paper.

3. DESIGN AND FABRICATION OF THE QUAD-BAND PATCH ANTENNA

The reduced-size patch antenna, whose design is developed as explained in Section 2, can be further modified to add additional resonances at 45, 51, and 56 GHz. To get the higher order resonances located at the desired frequency bands, it is suggested inserting reactively coupled elements of the appropriate geometry. For example, a secondary patch can be added as a parasitic radiator. The load impedance caused by such a reactively coupled patch controls the locations of the higher-order resonant frequencies.

Another approach to arrive at the final design of the quad-band patch antenna can be simply demonstrated as shown in Figure 6. The proposed antenna can be viewed as two overlapped rhombic patches as shown in Figure 6(a); the primary patch (on the left-hand) then cuts the secondary one, and a narrow gap is inserted between them as shown in Figure 6(b); some geometrical modifications are made to reduce the conducting area of the primary patch as previously described in Section 2, see Figures 6(c) and 6(d). The final geometry of the quad-band patch antenna is shown in Figure 6(d). This patch can be excited using either a probe feed, Figure 6(d), or a microstrip line. In this work, a microstrip line is used to excite the primary patch through an inset feed for impedance matching as shown in Figure 6(e). The secondary patch is fed via capacitive coupling to the primary edge.

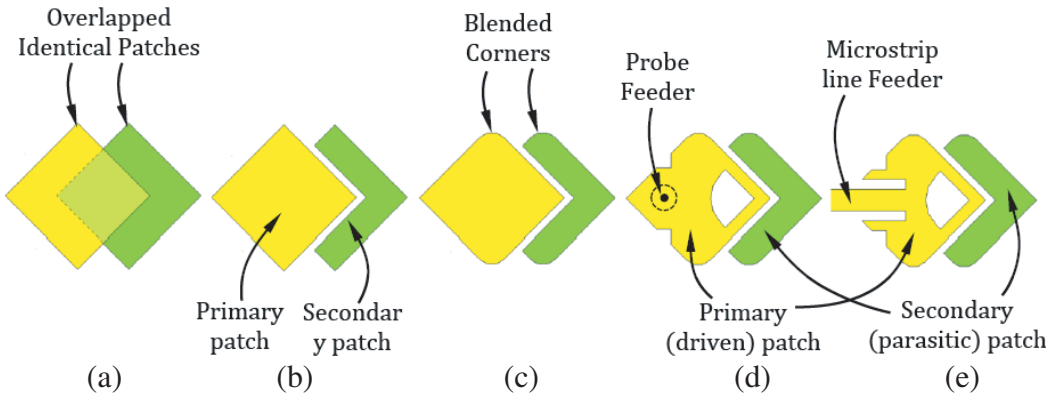

Figure 6. The antenna structure can be regarded as two overlapped rhombic patches with some geometrical modifications, done sequentially from (a) to (e), for impedance matching and good radiation characteristics at the principle resonant frequency (28 GHz) as well as the higher-order resonances (45, 51, and 56 GHz).

3.1. Construction of Quad-Band Patch Antenna

The geometry of the proposed quad-band antenna operating at 28, 45, 51, and 56 GHz bands with the final design is presented in Figure 7. The antenna structure can be viewed as composed of primary and secondary patches. The primary patch is responsible for radiation at 28 GHz and is excited through a microstrip line with inset feed. The secondary patch is capacitively coupled to the primary patch and can be considered as a parasitic radiator. The composite structure of the dual-patch antenna is responsible for radiation at the other three frequency bands around 45, 51, and 56 GHz. To allow the reduction of the substrate dimensions without excessive back radiation, the proposed antenna has solid ground plane without any defects in its structure.

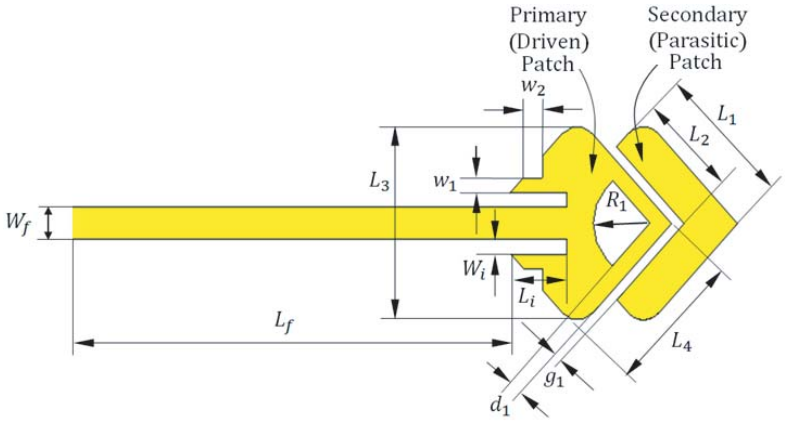

Figure 7. Final geometry of the proposed quad-band patch antenna.

The antenna is fabricated on a Rogers RO3003 substrate of height $h = 0.25$ mm, dielectric constant $\varepsilon_r = 3$, and loss tangent $\tan\delta = 0.001$. The substrate is placed over a solid ground plane. The feeding microstrip transmission line has a characteristic impedance of 50 Ω and dimensions of $W_f \times L_f$. An inset feed is used to match the antenna impedance to 50 Ω source.

Extensive parametric studies are performed through electromagnetic simulation for setting the optimum values of the dimensional parameters shown in Figure 7. For example, the side length of the rhombus-shaped primary patch, L_4, is the main parameter that determines the locations of the resonant frequencies for the four operational frequency bands of the proposed antenna. Changing L_4, results in changing the frequency response of $|S_{11}|$ as shown in Figure 8(a). For $L_4 = 3.02$, the four operational bands of the antenna are located at 28, 45, 51, and 56 GHz. Another important parameter is the inset length, L_I. As shown in Figure 8(b), the values of $|S_{11}|$ at the four resonant frequencies are strongly dependent on this parameter. For $L_I = 1.59$, all the values of $|S_{11}|$ at the four resonant frequencies are below −20 dB.

The optimum values of the symbolic dimensional parameters of the antenna, shown in Figure 7, are given in Table 1. At these parameter values, the proposed antenna has the optimum performance at the four operational frequency bands.

Table 1. Dimensions of the proposed antenna.

Dimension	L_1	L_2	L_3	L_4	w_1	w_2	W_i	L_i	W_f	L_f	g_1	d_1
Value (mm)	3.14	2.15	3.86	3.02	0.4	0.62	0.3	1.59	0.63	9.98	0.28	0.48

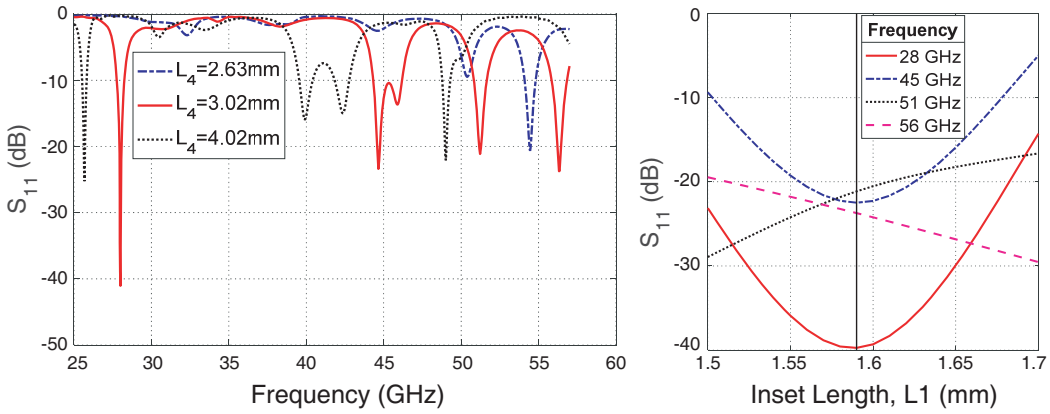

(a) (b)

Figure 8. Effect of the dimensional parameters. (a) Length of the primary patch, L_4, and (b) inset length, L_I, on the reflection coefficient S_{11} at the feeding port of the proposed antenna. The other diemnsional parameters are given in Table 1.

3.2. Numerical Simulation and Experimental Assessment of the Quad-Band Patch Antenna

This section is concerned with the presentation of the results of numerical simulation and experimental measurements of the proposed quad-band microstrip patch antenna. To confirm the accuracy of the assessed performance for both the single-element and MIMO antennas, the experimental measurements are compared to those obtained by electromagnetic simulation using the commercially available CST® software package. The prototype shown in Figure 9 is fabricated for this purpose. The antenna size is compared to the size of a coin of standard one-inch diameter. Excluding the feeder line, the outer dimensions of antenna are 4×5 mm.

Figure 9. Fabricated prototype of the proposed quad-band patch antenna with its size compared to a metal coin of standard size.

3.2.1. Reflection Coefficient at the Antenna Port

The vector network analyzer (VNA) of Rhode and Schwartz model ZVA67 is used for measuring the frequency response of the reflection coefficient magnitude $|S_{11}|$. The 1.85 mm end-launch connector from Southwest Microwave Inc. is used for connecting the antenna to the VNA as shown in Figure 10.

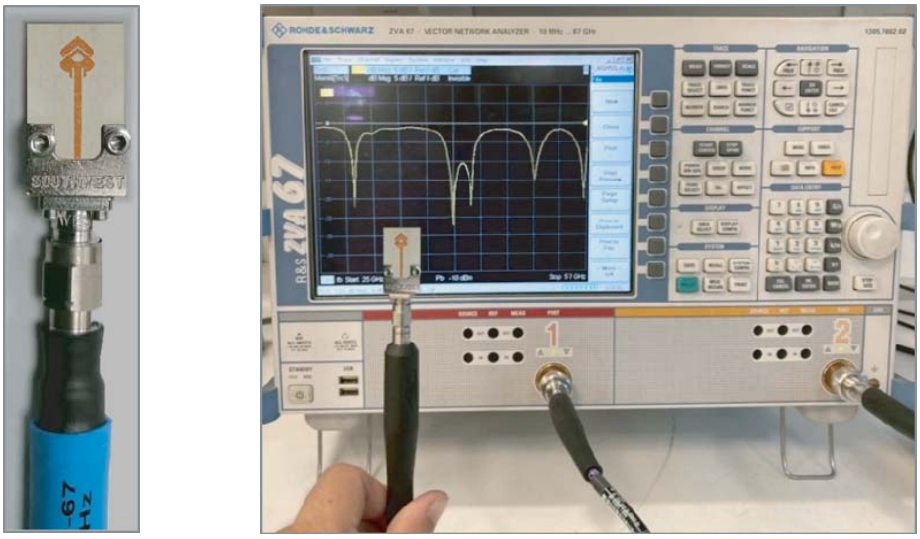

(a) (b)

Figure 10. Measurement of the reflection coefficient $|S_{11}|$ of the proposed quad-band patch antenna. (a) The fabricated prototype is connected to the end launcher, (b) the antenna is connected to the VNA of Rhode and Schwartz model ZVA67.

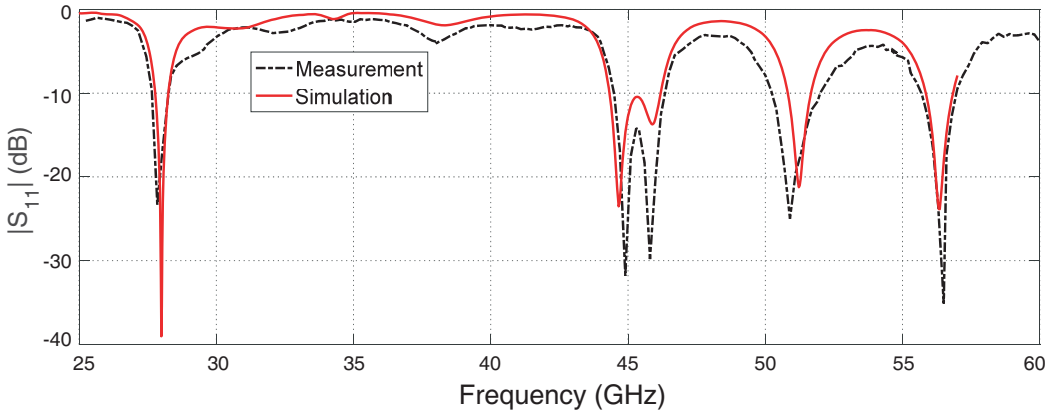

Figure 11. Dependence of the reflection coefficient $|S_{11}|$ of the frequency for the proposed quad-band patch antenna.

The numerical simulation and experimental measurements for the frequency dependence of the magnitude of the reflection coefficient, $|S_{11}|$ are presented in Figure 11. The experimental measurements show good agreement with the numerical results obtained by the CST simulator. It is clear that the antenna has excellent impedance matching over four frequency bands centered at 28, 45, 51, and 56 GHz where the value of $|S_{11}|$ is less than -20 dB with respect to 50 Ω feeder.

3.2.2. Radiation Patterns of the Quad-Band Patch Antenna

The experimental setup for measuring the radiation patterns and maximum gain of the proposed antenna is presented in Figure 12. The VNA Rhode and Schwartz model ZVA67 operating in the two-port measurement mode is used for this purpose by measuring the transmission coefficient $|S_{21}|$ through the antenna under test and the reference-gain linearly-polarized horn antennas models LB-018400 (for 18–

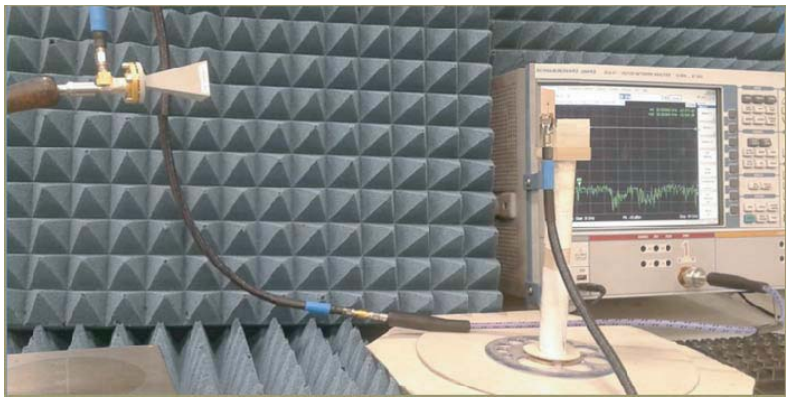

Figure 12. Experimental setup for measuring the radiation pattern and gain of the quad-band antenna.

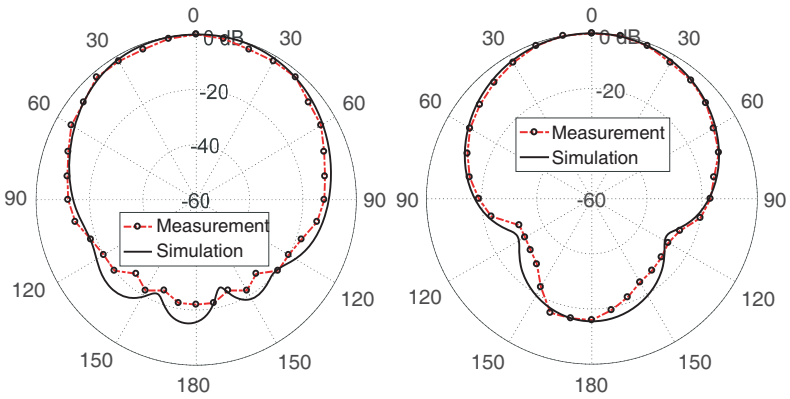

Figure 13. Radiation patterns of the proposed quad-band patch antenna in the elevation planes $\phi = 0°$ and $\phi = 90°$ at 28 GHz.

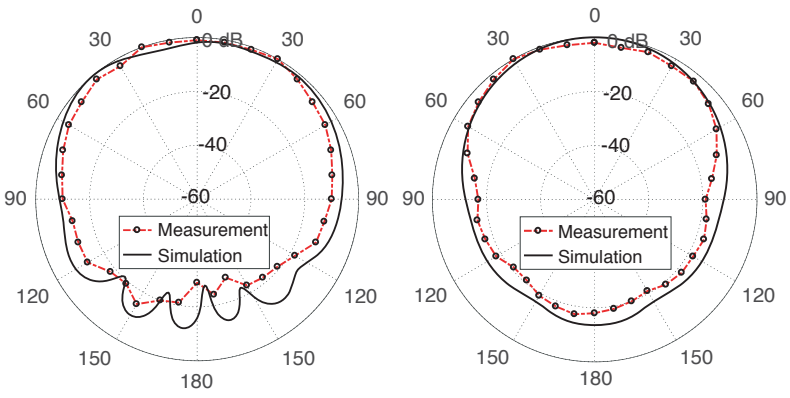

Figure 14. Radiation patterns of the proposed quad-band patch antenna in the elevation planes $\phi = 0°$ and $\phi = 90°$ at 45 GHz.

40 GHz band) and LB-12-10-A (for 40–60 GHz band). The radiation patterns of the proposed antenna at 28, 45, 51, and 56 GHz are presented in Figures 13, 14, 15, and 16, respectively, in the elevation planes $\phi = 0°$ and $\phi = 90°$. The experimental measurements show good agreement with the numerical results obtained by the CST simulation package. It is shown that the radiation patterns obtained at the four frequencies are acceptable and can be appropriate for either long-range or short-range communications.

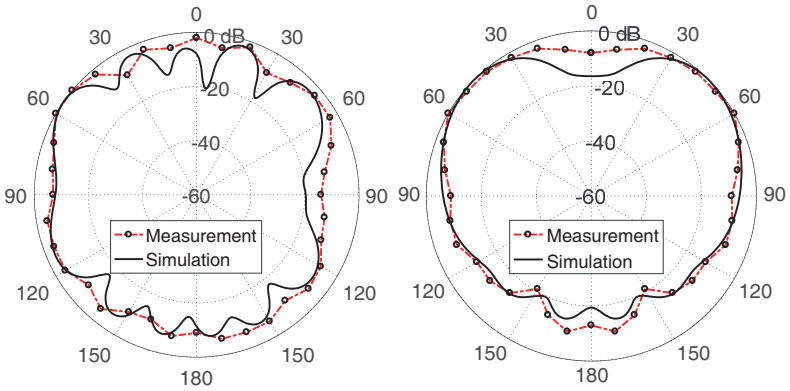

Figure 15. Radiation patterns of the proposed quad-band patch antenna in the elevation planes $\phi = 0°$ and $\phi = 90°$ at 51 GHz.

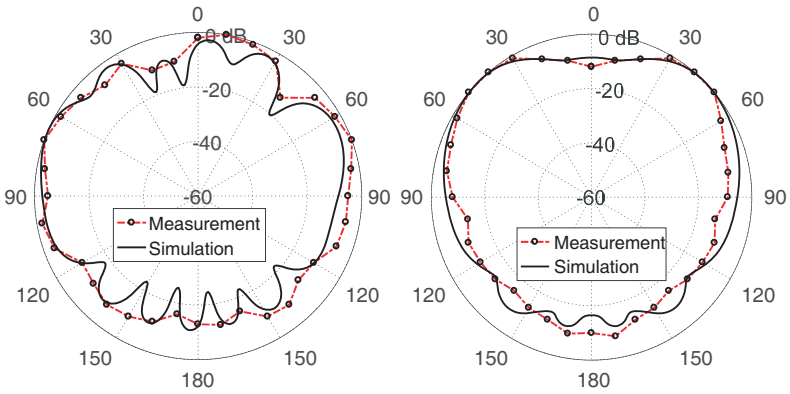

Figure 16. Radiation patterns of the proposed quad-band patch antenna in the elevation planes $\phi = 0°$ and $\phi = 90°$ at 56 GHz.

4. MIMO ANTENNA SYSTEMS USING THE QUAD-BAND PATCH ANTENNA

In this section, two-port and four-port MIMO antenna systems are constructed using the quad-band patch antenna. Prototypes of the proposed MIMO antennas are fabricated for the purpose of experimental assessment. The results of numerical simulation are compared to those of experimental measurements for the purpose of confirmation.

4.1. Two-Port MIMO Antennas Using the Quad-Band Patch Antenna

Prototypes are fabricated for two-port MIMO antenna systems constructed as two elements of the proposed quad-band patch antenna using different configurations. The patches of the first MIMO system are arranged side-by-side as shown in Figure 17(a). The patches of the other MIMO system are arranged face-to-face as shown in Figure 18(a). A prototype is fabricated for each type of the MIMO antenna systems as shown in Figures 17(b) and 18(b), respectively, and connected to a coaxial feeder using coaxial end launchers for experimental assessment. The VNA of Rhode and Schwartz model ZVA67 is used to evaluate the transmission coefficient $|S_{21}|$ for the fabricated prototypes of the proposed MIMO antennas.

The frequency dependence of the coupling coefficient $|S_{21}|$ for each of the two-port MIMO configurations is presented in Figure 19. The experimental measurements show good agreement with the simulation results, and both of them show that the antennas of each MIMO configuration are very weakly coupled where $|S_{21}|$ does not exceed -25 dB over the entire frequency range. It is clear that the

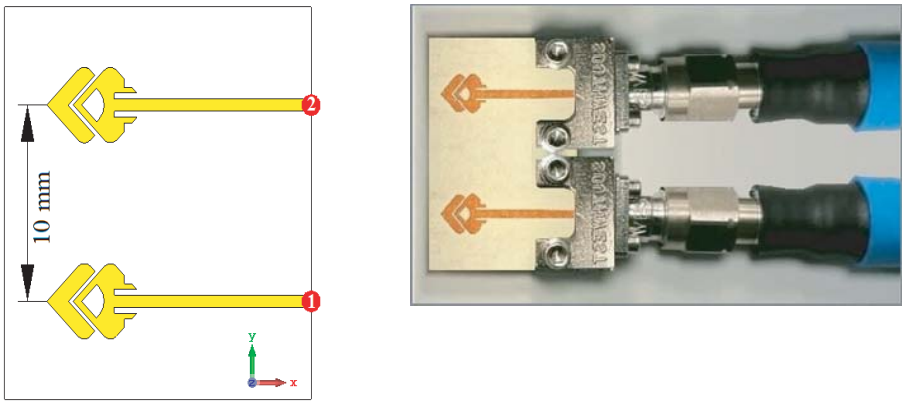

(a) (b)

Figure 17. Two-port MIMO antenna system constructed as two elements of the quad-band patch arranged side-by-side. (a) Model in the CST simulator, (b) fabricated prototype is connected to end launchers and coaxial cables for measurements.

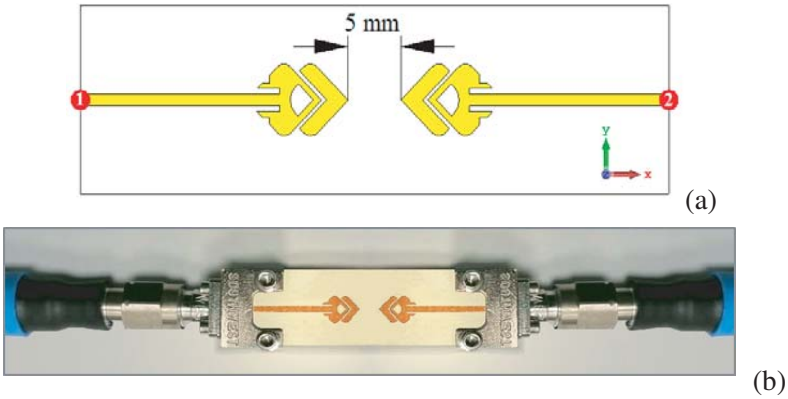

(a)

(b)

Figure 18. Two-port MIMO antenna system constructed as two elements of the quad-band patch arranged face-to-face. (a) Model in the CST simulator, (b) fabricated prototype is connected to end launchers and coaxial cables for measurements.

coupling coefficients, S_{21}, of the face-to-face MIMO configuration have larger magnitudes than those of the side-by-side MIMO configuration. This can be attributed to that the face-to-face configuration has narrower separation between the two antennas than that in the side-by-side configuration. Moreover, the face-to-face configuration allows higher rate of power transfer between the two antennas of the MIMO system because each antenna lies in the direction of the power flowing on the transmission line feeding the other antenna.

4.2. Four-Port MIMO Antenna System

To construct a four-port MIMO antenna system for operation at 28, 45, 51, and 56 GHz, four elements of the quad-band microstrip patch antenna with the dimensions listed in Table 1 are arranged as shown in the geometric model presented in Figure 20 for the MIMO antenna in the CST simulator. The separations among the four antennas are set so as to achieve the spatial diversity required for the target 5G applications. This design has the total dimensions of $42 \times 20\,\text{mm}^2$. Such a MIMO antenna system can be practically suitable to be manufactured and integrated on a printed electronic board of a mobile handset.

The prototype shown in Figure 21 is fabricated for the purpose of experimental assessment of

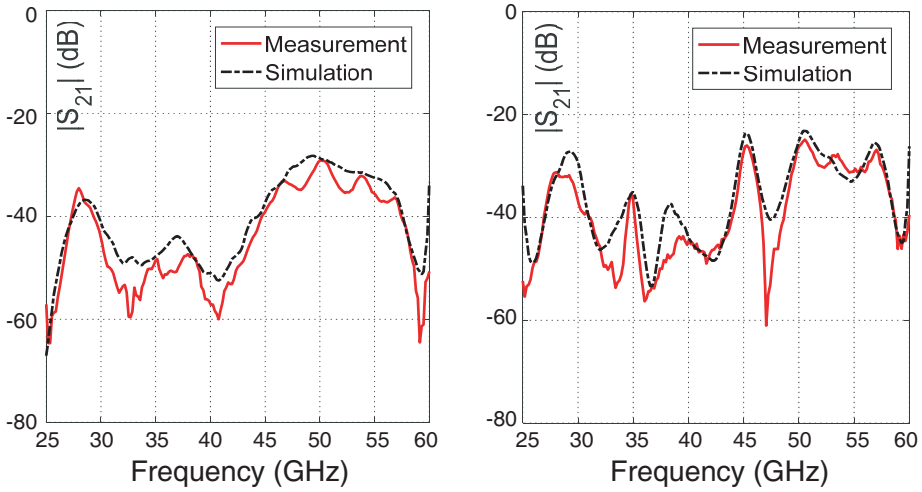

Figure 19. Frequency responses of the coupling coefficient $|S_{21}|$ for the two-port MIMO configurations. (a) Side-by-Side configuration shown in Figure 17, (b) face-to-face configuration shown in Figure 18.

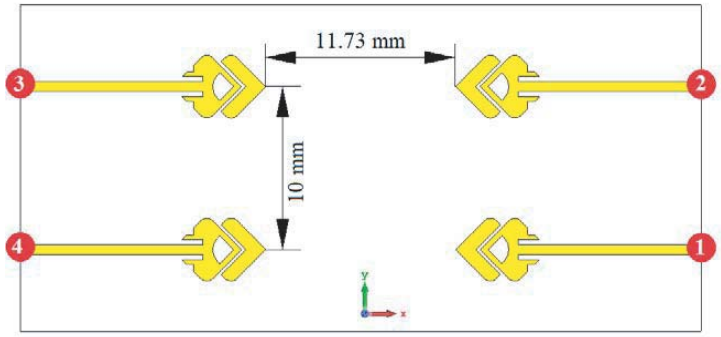

Figure 20. Design of the quad-band four-port MIMO antenna system (total dimensions $42 \times 20\,\text{mm}^2$) proposed for mobile handsets.

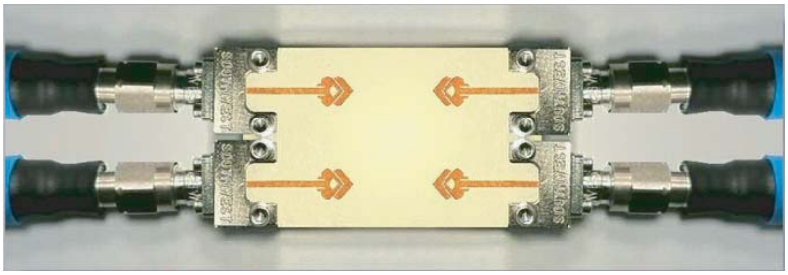

Figure 21. Fabricate quad-band four-port MIMO antenna system.

the performance of the proposed quad-band four-port MIMO antenna system. The VNA Rhode and Schwartz model ZVA67 is used for measuring the frequency response of the reflection coefficients S_{21}, S_{43}, S_{31}, S_{42}, S_{41}, and S_{32}. Four 1.85 mm end-launch connectors from Southwest Microwave Incorporation are used for connecting the corresponding antenna ports to the VNA whereas the other two ports are connected to matched ($50\,\Omega$) loads as shown in Figure 21.

4.2.1. Coupling Coefficients, Envelop Correlation Coefficients, and Diversity Gain

The simulation results and experimental measurements describing the frequency dependence of the magnitudes of the scattering parameters S_{21}, S_{43}, S_{31}, S_{42}, S_{41}, and S_{32} representing the different coupling coefficients for the proposed quad-band four-port MIMO antenna system are presented in Figure 22. The simulation results appear in agreement with the results of the experimental measurements, and both of them show low values of the coupling coefficients.

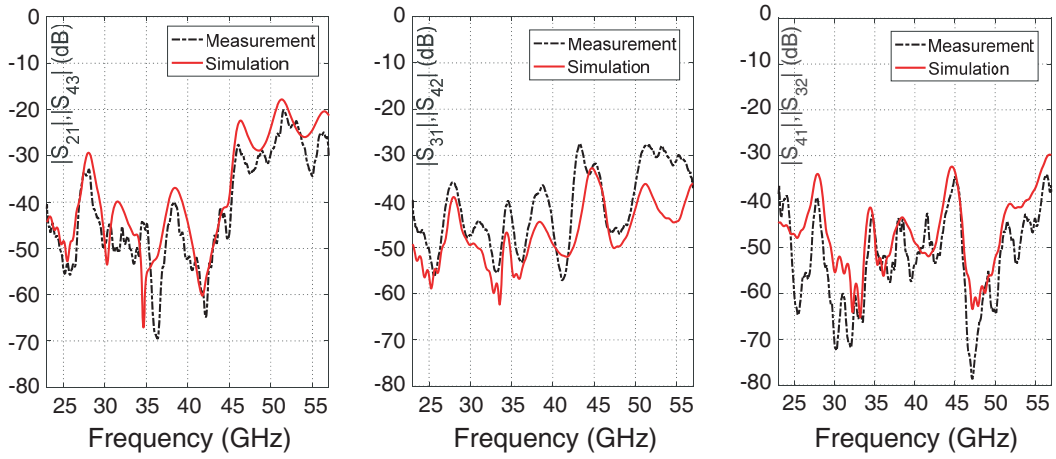

Figure 22. Frequency dependence of the magnitudes of the scattering parameters S_{21}, S_{43}, S_{31}, S_{42}, S_{41}, and S_{32} representing the different coupling coefficients for the proposed quad-band four-port MIMO antenna system.

The dependencies of the ECC and the DG of the proposed four-port MIMO antenna system on the frequency are presented in Figure 23. It is shown that at the operating frequencies 28, 45, 51, and 56 GHz and over the width of each of the four bands, the ECC is very low (almost 0), and consequently, the DG is very high (almost 10). This can be considered as the optimum performance of MIMO antenna system. It should be noted that the relative positions of the antennas in the pair of ports (1,2) are the same as those in the pair of ports (3,4); this leads to identical ECC and DG as shown in Figure 22. The same applies to antenna pairs (1,3) and (2,4) and, also, for antenna pairs (1,4) and (2,3).

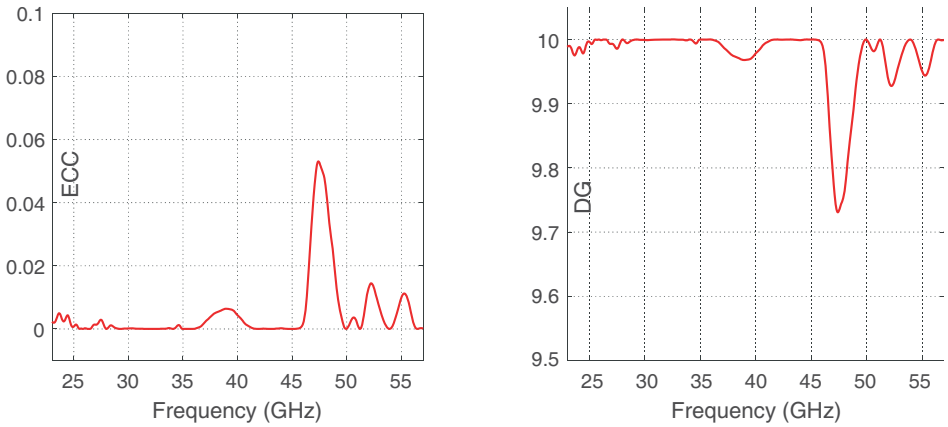

Figure 23. Dependence of the ECC and DG on the frequency for the proposed quad-band four-port MIMO antenna system for ports (1,2) and (3,4).

4.2.2. Radiation Patterns of the Four-Port MIMO Antenna System

The radiation patterns produced at 28, 45, 51, and 56 GHz by the four-port MIMO antenna system, shown in Figure 21, are presented in Figures 24, 25, 26, and 27, respectively, when the MIMO antenna system is excited at different ports. The radiation patterns appear suitable for most of the future wireless applications relevant to the mobile handsets. More specifically, the radiation patterns produced at 28 and 45 GHz are ripple-free and appear appropriate for long-range cellular mobile networks. On the other hand, the radiation patterns at 51 and 56 GHz have some ripples and may be more appropriate for short-range communications.

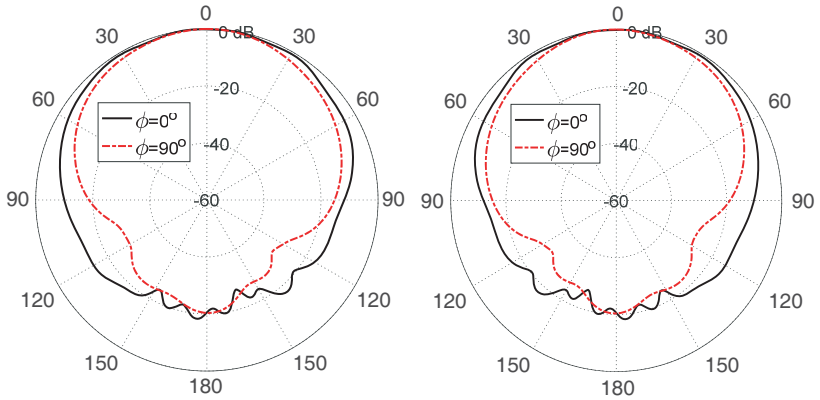

Figure 24. Radiation patterns in the elevation planes for the quad-band MIMO antenna system at 28 GHz when excited at the indicated ports.

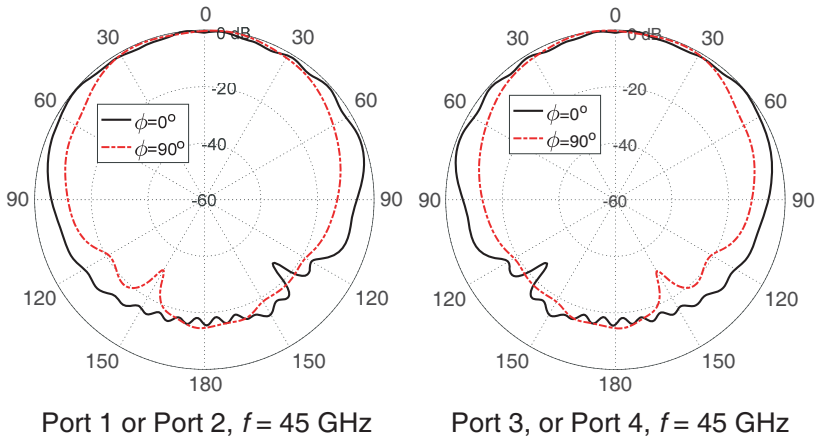

Figure 25. Radiation patterns in the elevation planes for the quad-band MIMO antenna system at 45 GHz when excited at the indicated ports.

5. SUMMARY OF THE PROPOSED ANTENNA PERFORMANCE

This section is concerned with providing a summary of the most important performance metrics for the quad-band patch antenna as well as the MIMO antenna systems proposed in the present work.

Table 2 gives a summary of the single-element as well as the MIMO antenna performance at the four operational frequencies. Table 3 gives comparative performance among some mm-wave patch antennas available in some recent literature and the antenna proposed in the present work.

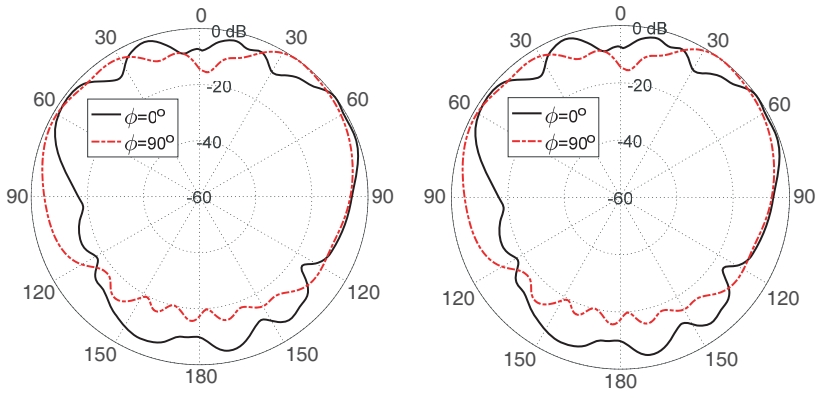

Figure 26. Radiation patterns in the elevation planes for the quad-band MIMO antenna system at 51 GHz when excited at the indicated ports.

Table 2. Achieved frequency bands (obtained experimentally) by the proposed quad-band patch antenna and the corresponding gain and radiation efficiency.

Center Frequency (GHz)	Start Frequency (GHz)	End Frequency (GHz)	Bandwidth (GHz)	Gain (dBi)	Radiation Efficiency
28	27.70	28.30	0.60	7.30	86.5%
45	44.50	46.50	2.00	7.03	87.5%
51	50.20	52.00	1.80	7.20	89.2%
56	55.70	57.00	1.30	8.03	90.0%

Table 3. Comparison with other published designs of mm-wave antennas.

Work	Center Frequencies (GHz)	Gain (dBi)	Patch Dimensions (mm^2)	-10 dB BW (GHz)	Envelope Correlation Coefficient (ECC)	DG
[9]	28 38	7.2 9.2	4.6×2.8	1.07 1.43	7.65	NA
[13]	28 38	3.7 5.1	3.7×5.1	3.3 1.4	NA	NA
[1]	38 45	7.6 7.2	6.0×6.0	1.2 0.92	NA	NA
[11]	38 54	6.9 7.4	6.3×6.0	1.94 2.0	NA	NA
[Present]	28 45 51 56	7.3 7.03 7.2 8.03	4.0×5.0	0.5 1.8 0.8 1.0	1.4 9.5 2	> 9.99

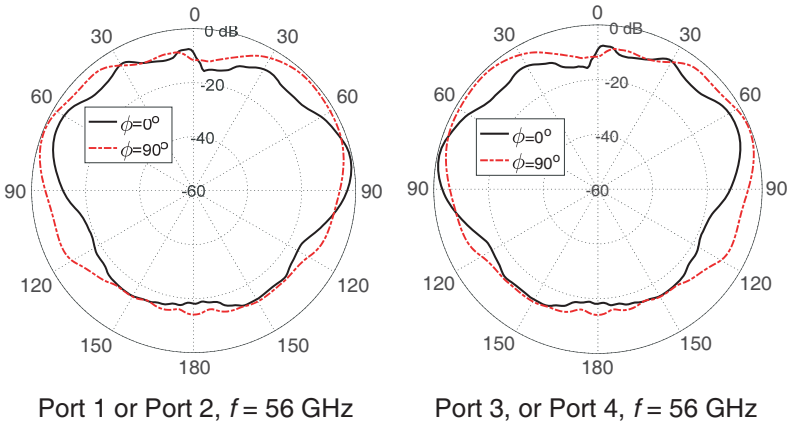

Figure 27. Radiation patterns in the elevation planes for the quad-band MIMO antenna system at 56 GHz when excited at the indicated ports.

6. CONCLUSION

A novel design for a compact-size quad-band microstrip patch antenna is introduced for the 5G mobile communications in the frequency bands 28, 45, 51, and 56 GHz. A new method is described to reduce the size of a 28-GHz rhombic patch antenna so as to properly operate at the higher frequency bands (45/51/56 GHz) without negative effects on the antenna characteristics at 28 GHz. The proposed quad-band antenna has primary and secondary patches which are reactively coupled and well designed to produce appropriate radiation patterns and good impedance matching in the four frequency bands of operation. Two-port and four-port MIMO antenna systems that employ the quad-band microstrip patch are investigated for operation in the 5G mobile handsets. The performance of both the quad-band patch antenna and the MIMO antenna systems are assessed including the return loss at each antenna port and the coupling coefficients between the different ports. It is shown that the simulation results agree with the experimental measurements, and both show good performance. The bandwidths achieved around 28, 45, 51, and 56 GHz are, respectively, 0.6, 2.0, 1.8, and 1.3 GHz. It is shown that the ECC and the DG are perfect over the four frequency bands for the four-port MIMO antenna system.

REFERENCES

1. Khattak, M. I., A. Sohail, U. Khan, Z. Barki, and G. Witjaksono, "Elliptical slot circular patch antenna array with dual band behaviour for future 5G mobile communication networks," *Progress In Electromagnetics Research C*, Vol. 89, 133–147, 2019.
2. Şeker, C., T. Ozturk, and M. T. Güneşer, "A single band antenna design for future millimeter wave wireless communication at 38 GHz," *European Journal of Engineering and Formal Sciences*, Vol. 2, No. 2, 35–39, 2018.
3. Saini, J. and S. K. Agarwal, "Design a single band microstrip patch antenna at 60 GHz millimeter wave for 5G application," *2017 international conference on Computer, Communications and Electronics (Comptelix)*, 227–230, IEEE, 2017.
4. Hong, W., K.-H. Baek, and S. Ko, "Millimeter-wave 5G antennas for smartphones: Overview and experimental demonstration," *IEEE Transactions on Antennas and Propagation*, Vol. 65, No. 12, 6250–6261, 2017.
5. Andrews, J. G., S. Buzzi, W. Choi, S. V. Hanly, A. Lozano, A. CK Soong, and J. C. Zhang, "What will 5G be?," *IEEE Journal on Selected Areas in Communications*, Vol. 32, No. 6, 1065–1082, 2014.
6. Farahat, A. E. and K. F. A. Hussein, "28/38 GHz dual-band Yagi-Uda antenna with corrugated radiator and enhanced reflectors for 5G MIMO antenna systems," *Progress In Electromagnetics Research C*, Vol. 101, 159–172, 2020.

7. Varzakas, P., "Average channel capacity for rayleigh fading spread spectrum MIMO systems," *International Journal of Communication Systems*, Vol. 19, No. 10, 1081–1087, Dec. 2006.
8. Wani, Z., M. P. Abegaonkar, and S. K. Koul, "A 28-GHz antenna for 5G MIMO applications," *Progress In Electromagnetics Research Letters*, Vol. 78, 73–79, 2018.
9. Marzouk, H. M., M. I. Ahmed, and A.-E. H. Shaalan, "Novel dual-band 28/38 GHz MIMO antennas for 5G mobile applications," *Progress In Electromagnetics Research C*, Vol. 93, 103–117, 2019.
10. Sharaf, M. H., A. I. Zaki, R. K., Hamad, and M. M. Omar, "A novel dual-band (38/60 GHz) patch antenna for 5G mobile handsets," *Sensors*, Vol. 20, No. 9, 2541, 2020.
11. Imran, D., M. M. Farooqi, M. I. Khattak, Z. Ullah, M. I. Khan, M. A. Khattak, and H. Dar, "Millimeter wave microstrip patch antenna for 5G mobile communication," *2018 International Conference on Engineering and Emerging Technologies (ICEET)*, 1–6, IEEE, 2018.
12. Lin, H.-S. and Y.-C. Lin, "Millimeter-wave MIMO antennas with polarization and pattern diversity for 5G mobile communications: The corner design," *2017 IEEE International Symposium on Antennas and Propagation & USNC/URSI National Radio Science Meeting*, 2577–2578, IEEE, 2017.
13. Ahmad, W. and W. T. Khan, "Small form factor dual band (28/38 GHz) PIFA antenna for 5G applications," *2017 IEEE MTT-S International Conference on Microwaves for Intelligent Mobility (ICMIM)*, 21–24, IEEE, Mar. 2017.